

Anomalous minimum in the shear viscosity of a Fermi gas

E. Elliott^{1,2}, J. A. Joseph¹, and J. E. Thomas¹

¹*Department of Physics, North Carolina State University, Raleigh, NC 27695, USA and*

²*Department of Physics, Duke University, Durham, NC 27708, USA*

(Dated: March 2, 2019)

We measure the static shear viscosity η in a two-component Fermi gas near a broad collisional (Feshbach) resonance, as a function of interaction strength and energy. We find that η has both a quadratic and a linear dependence on the interaction strength $1/(k_{FI}a)$, where a is the s-wave scattering length and k_{FI} is the Fermi wave vector for an ideal gas at the trap center. At low energy, the minimum is less than the resonant value and is significantly shifted toward the BEC side of resonance, to $1/(k_{FI}a) = 0.2$.

PACS numbers: 03.75.Ss

Ultra-cold Fermi gases provide a unique model for studying the properties of strongly interacting quantum fluids [1–5]. Utilizing a collisional (Feshbach) resonance, a bias magnetic field readily tunes interactions between spin-up and spin-down atoms from non-interacting to strongly repulsive or strongly attractive [6]. Several ground-breaking measurements have focused on the equilibrium thermodynamic properties [7–11]. However, systematic study of interaction-dependent hydrodynamic transport coefficients poses new challenges. Measurement of the shear viscosity is of particular interest in recent predictions [12–15] and in the context of a “perfect” fluid conjecture [16], derived using holographic duality methods [5]. The conjecture states that for a broad class of (conformal) strongly interacting quantum fields, the ratio of the shear viscosity η to the entropy density s has a universal minimum, $\eta/s \geq \hbar/(4\pi k_B)$ [16]. Recent measurements of the shear viscosity for a resonantly interacting Fermi gas [17, 18] yield a minimum η/s ratio just 4.5 times the lower bound, comparable to that of a quark-gluon plasma [5]. Whether the shear viscosity of a Fermi gas (or the η/s ratio) is minimized at resonance or at a finite scattering length is an open question.

In this Letter, we describe a measurement of the shear viscosity η for Fermi gas as a function of the s-wave scattering length a and energy near a broad Feshbach resonance. We show that high sensitivity to the shear viscosity is obtained by releasing the cloud from an asymmetric optical trap and measuring the transverse aspect ratio as a function of time after release. We determine the leading order, finite a correction to the shear viscosity as a function of $1/(k_{FI}a)$ and energy, where k_{FI} is the Fermi wavevector of an ideal gas at the trap center. In kinetic theory, η is expected to scale as $1/(k_{FI}a)^2$. However, we find that for the energy range measured in the experiments, there is an additional linear dependence on $1/(k_{FI}a)$, which decreases with increasing energy, while the quadratic dependence remains nearly constant. This results in a shift of the minimum viscosity toward the BEC side of resonance at low energy. The minimum viscosity is found to be slightly less than that at resonance, for which new measurements are presented.

In the experiments, we employ an optically-trapped

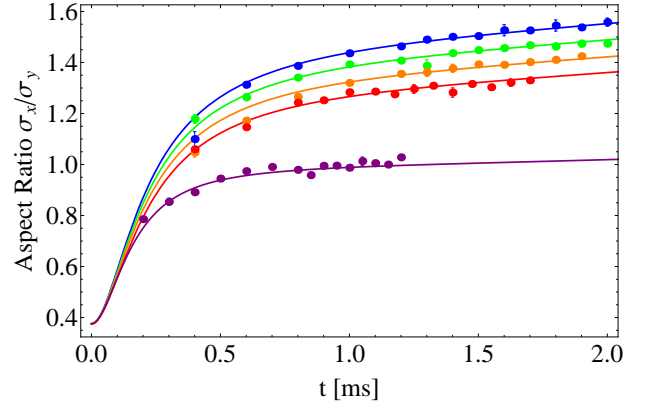


FIG. 1: Transverse aspect ratio σ_x/σ_y versus time after release showing elliptic hydrodynamic flow: Top to bottom: Resonantly interacting gas at 834 G, $E = 0.52 E_F$, $E = 0.75 E_F$, $E = 0.96 E_F$, $E = 1.66 E_F$, ballistic gas at 528 G, $E = 1.78 E_F$. Top four solid curves: Hydrodynamic theory with the shear viscosity as the only fit parameter; Lower solid curve: Ballistic theory with no free parameters. Error bars denote statistical fluctuations.

Fermi gas of ${}^6\text{Li}$ atoms in a 50-50 mixture of the two lowest hyperfine states, which is tuned near a broad Feshbach resonance and cooled by evaporation [1]. An asymmetric trap is employed in these experiments, with a 1:2.7:33 (x:y:z) aspect ratio, as determined from the harmonic oscillation frequencies of atoms, measured by parametric resonance and corrected for trap anharmonicity. For the optical trap potential U_{opt} : $\omega_x = 2\pi \times 2210(4)$ Hz, $\omega_y = 2\pi \times 830(2)$ Hz, and $\omega_{zopt} = 2\pi \times 60.7(0.1)$ Hz. Curvature in the bias magnetic field introduces an additional magnetic potential $U_{mag} = \frac{1}{2}m\omega_{mag}^2(y^2 + z^2 - 2x^2)$, where m is the ${}^6\text{Li}$ mass and $\omega_{mag} = 2\pi \times 21.5(0.25)\sqrt{B/834}$ Hz is the oscillation frequency of the cloud along the y -axis, which is measured at 834 G with $U_{opt} = 0$. For later use, we define the ideal gas Fermi energy $E_F \equiv (3N)^{1/3}\hbar\bar{\omega}$, and the corresponding wavevector $k_{FI} = (2mE_F/\hbar^2)^{1/2}$, where N is the total number of atoms, $\bar{\omega} = (\omega_x\omega_y\omega_z)^{1/3}$ and $\omega_z = (\omega_{zopt}^2 + \omega_{mag}^2)^{1/2}$.

After evaporative cooling, the interaction strength is

adjusted by tuning the bias magnetic field. Then the optical trap is extinguished and the cloud radii are measured as a function of time after release in all three dimensions, using two simultaneous probe pulses interacting with different spin states to obtain independent absorption images on two CCD cameras. The magnifications of the cameras are calibrated by moving the focus of the optical trap and comparing the common z-direction measurements, which agree to within 1% for an average over many shots. Then the effective magnification of one camera is adjusted so that the average z-cloud radii are identical, to assure that the aspect ratios are consistently measured. At resonance, the energy E is given by the virial theorem in terms of the cloud profile [8, 19]. However, at finite scattering length, the energy of the cloud does not have a simple relation to the cloud profile. Instead, we employ a measurement of $\tilde{E} \equiv \langle \mathbf{r} \cdot \nabla U \rangle_0$, where $U = U_{opt} + U_{mag}$ as defined above. \tilde{E} is independent of the scattering length and equal to twice the potential energy in a harmonic trap.

Measurement of the shear viscosity is accomplished with high sensitivity by measuring the transverse (x:y) aspect ratio of the cloud after release from the trap, Fig. 1. As the initial x:y aspect ratio of the cloud is 1:2.7 for our trap, the cloud exhibits elliptic flow in the x-y plane. The shear viscosity pressure tensor slows the flow in the initially narrow, rapidly expanding, x-direction and transfers energy to the more slowly expanding y-direction. For a fixed time after release, the transverse aspect ratio σ_x/σ_y then decreases with increasing shear viscosity. In contrast to measurements employing the axial z-direction, which expands slowly, the relatively high frequencies ω_x and ω_y assure that σ_x/σ_y saturates on a rapid time scale, where the expanded cloud images still have high signal to background ratio, and reduces sensitivity to the magnetic potential. For a non-interacting ballistic gas at 528 G, we observe that σ_x/σ_y saturates to unity, while for the resonantly interacting cloud at 834 G, which expands hydrodynamically, σ_x/σ_y exceeds 1.5. This limiting condition is clearly observable and exhibits energy dependence, which arises from the shear viscosity.

The shear viscosity is given in natural units of $\hbar n$ by $\eta \equiv \alpha \hbar n$, where α is a dimensionless shear viscosity coefficient. The trap-averaged shear viscosity coefficient is then defined as

$$\bar{\alpha}_S \equiv \frac{1}{N\hbar} \int d^3\mathbf{r} \eta = \frac{1}{N} \int d^3\mathbf{r} n \alpha \quad (1)$$

At resonance, where $a^{-1} = 0$, α can be a function only of the local reduced temperature θ . Then, with an adiabatic approximation for the temperature, θ remains fixed, and $\bar{\alpha}_S \equiv \bar{\alpha}_{S0}$ is temporally constant as the cloud expands. For finite large scattering length, we assume that the leading order correction to the local viscosity is symmetric in a and takes the form $\hbar n f_2(\theta)/(k_F a)^2$. Then, in a scaling approximation, where the density decreases by the volume scale factor Γ as the cloud expands (see below), $1/k_F^2 \propto \Gamma^{2/3}(t)$. Integrating over the cloud volume,

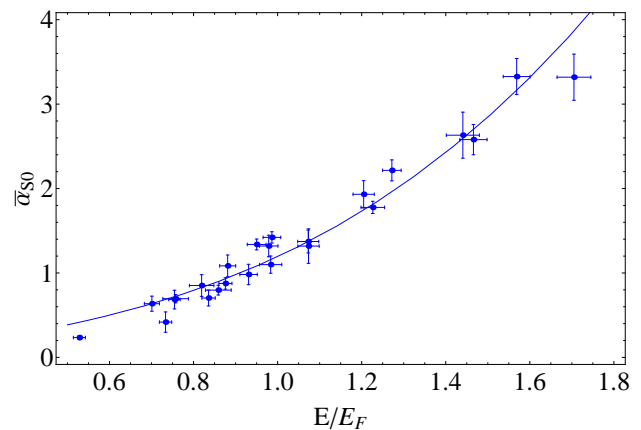


FIG. 2: Shear viscosity at resonance (834 G) in units of $\hbar n$, with n the density, versus energy E for $E/E_F < 2.0$. $\bar{\alpha}_{S0}$ is the trap-averaged shear viscosity coefficient from the fit using Eq. A32. E_F is the Fermi energy of an ideal gas at the trap center. The solid blue curve shows the fit $0.63 E/E_F + 0.56 (E/E_F)^3$ to the $E/E_F < 2.0$ data.

we can write

$$\bar{\alpha}_S(t) = \bar{\alpha}_{S0} + \bar{\alpha}_{S2} \Gamma^{2/3}(t), \quad (2)$$

where the first term is the contribution at resonance and the second term is the finite $1/a$ -dependent correction.

We determine the trap-averaged shear viscosity coefficients $\bar{\alpha}_{S0}$ and $\bar{\alpha}_{S2}$ by fitting a hydrodynamic theory in a scaling approximation to the measured cloud aspect ratios versus time after the optical trapping potential U_{opt} is extinguished (with U_{mag} remaining). In a scaling approximation, the expansion factors b_x, b_y, b_z for the cloud radii obey [20],

$$\ddot{b}_i = \frac{\overline{\omega_i^2}}{\Gamma^{2/3} b_i} [1 + C(t)] - \frac{\hbar \bar{\alpha}_S(t) \sigma_{ii}}{m \langle x_i^2 \rangle_0 b_i} - \omega_{imag}^2 b_i. \quad (3)$$

Here, $\Gamma(t) \equiv b_x b_y b_z$ is the volume scale factor and σ_{ii} is the shear viscosity stress tensor, which is traceless. Γ and σ_{ii} are functions only of the time in the scaling approximation, where the velocity field is linear in the spatial coordinates. We ignore the contribution of the bulk viscosity, which is found to be much smaller than the shear viscosity [20, 21]. In Eq. A32, we have defined the mean square ballistic frequency $\overline{\omega_i^2}$ for an arbitrary trapping potential, which need not be harmonic [20]. For the magnetic potential, $\omega_{ymag}^2 = \omega_{zmag}^2 = \omega_{mag}^2$ and $\omega_{xmag}^2 = -2\omega_{mag}^2$ (repulsive), with ω_{mag} defined above.

The coefficient $C(t) = C_Q(t) + C_{\Delta p}(t)$ in Eq. A32 includes the effects of heating in C_Q , which arises from the shear and bulk viscosities. $C_{\Delta p}(t)$ describes the effect of the conformal symmetry breaking pressure change $\Delta p \equiv p - \frac{2}{3} \mathcal{E}$, where p is the pressure and \mathcal{E} is the local energy density. Note that Δp vanishes at resonance [20]. We find that C_Q is important, but that $C_{\Delta p}$ has negligible effect on the transverse aspect ratio [20], although it significantly affects the mean square cloud radius [21].

The shear viscosity coefficients $\bar{\alpha}_{S0}$ and $\bar{\alpha}_{S2}$ in Eq. 2 are determined using Eq. A32 to fit the data for the transverse aspect ratio $\sigma_x/\sigma_y = \omega_y b_x/(\omega_x b_y)$ as a function of time after release, for the energy range $0.5 < E/E_F < 2.0$. We start with the resonant gas at 834 G. Using $\bar{\alpha}_{S0}$ as the only free parameter, we obtain $\bar{\alpha}_{S0}$ as a function of the initial energy per particle $E = \langle U \rangle_0 + \frac{1}{2} \langle \mathbf{r} \cdot \nabla U \rangle_0$ [8, 19], Fig. 2. Fitting the data with $c_1 E/E_F + c_3 (E/E_F)^3$, we find $c_1 = 0.63(0.08)$ and $c_3 = 0.56(0.06)$. Extrapolating the fit (without changing c_1 or c_3) for energies up to $E/E_F = 4.6$, we find very good agreement with the high energy data from Ref. [17, 18], as shown in Fig. 3. The very good fit over the whole energy range nicely demonstrates universal scaling, as the low energy data is taken using a shallow trap with a 1:2.7:33 aspect ratio and the high energy data is taken in a cylindrically symmetric trap that is 50 times deeper.

We note that the shear viscosity measured using collective mode damping in Ref. [17, 18] is systematically higher than that of the new data [20], where the transverse aspect ratio of an expanding gas is measured. Collective mode measurements measure the viscosity at the collective mode frequency in a trapped cloud, where the system becomes ballistic as the relaxation time increases with increasing energy. In contrast, expansion measurements eliminate the trap and measure the viscosity during a relatively long expansion time. This corresponds to a low frequency, where local thermodynamic equilibrium is more easily maintained. Further, for collective mode measurements at nonzero temperature, excess mode damping may arise from the cloud edges, where ballistic and hydrodynamic components vibrate out of phase.

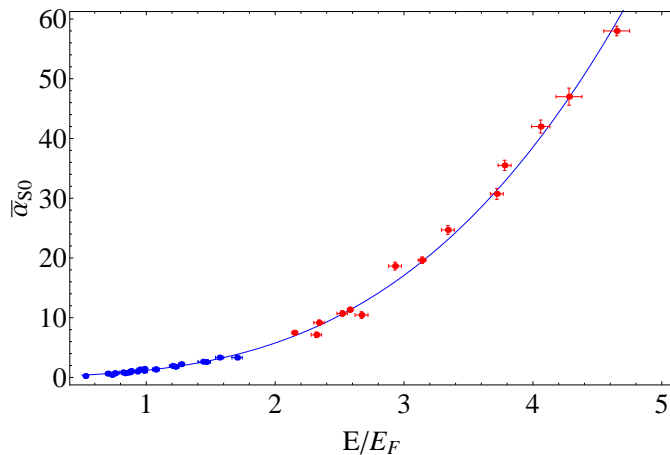


FIG. 3: Shear viscosity at resonance in units of $\hbar n$, with n the density, versus energy E . $\bar{\alpha}_{S0}$ is defined as in Fig. 2. Blue circles for $E/E_F < 2.0$ show data from fits to the transverse aspect ratio (this paper). Red circles for $E/E_F > 2.0$ show data from Ref. [17, 18]. The solid curve shows that the fit $0.63 E/E_F + 0.56 (E/E_F)^3$, obtained using only the low energy $E/E_F < 2.0$ data, is in very good agreement with the high energy $E/E_F > 2.0$ data.

Next, we measure the scattering-length dependent viscosity coefficient $\bar{\alpha}_{S2}$ in Eq. 2. For this measurement, we refit the $\bar{\alpha}_{S0}$ data as a function of the scattering-length-independent energy scale $\tilde{E} \equiv \langle \mathbf{r} \cdot \nabla U \rangle_0$, described above. From the fit, we obtain $\bar{\alpha}_{S0}(\tilde{E}) = 0.61(0.08) \tilde{E}/E_F + 0.62(0.06) (\tilde{E}/E_F)^3$. This polynomial for $\bar{\alpha}_{S0}(\tilde{E})$ at resonance is used as a known input in Eq. 2. Then, the transverse aspect ratio for data above and below resonance is fit using Eq. A32 with $\bar{\alpha}_{S2}$ as the only free parameter. Fig. 4 shows data obtained for different interaction strengths $1/(k_{FI}a)$, as a function of \tilde{E} . On resonance $\bar{\alpha}_{S2} = 0$ by construction. We use a linear fit to parameterize the energy dependence of $\bar{\alpha}_{S2}$ for each $1/(k_{FI}a)$. There is a clear increase in $\bar{\alpha}_{S2}$ with increasing energy below resonance ($1/(k_{FI}a) > 0$). Tuning closer to resonance, we see that the slope of the fitted line decreases. Above resonance ($1/(k_{FI}a) < 0$), the sign of the energy dependence is reversed and $\bar{\alpha}_{S2}$ decreases in magnitude with increasing energy. Using the linear fit to the energy

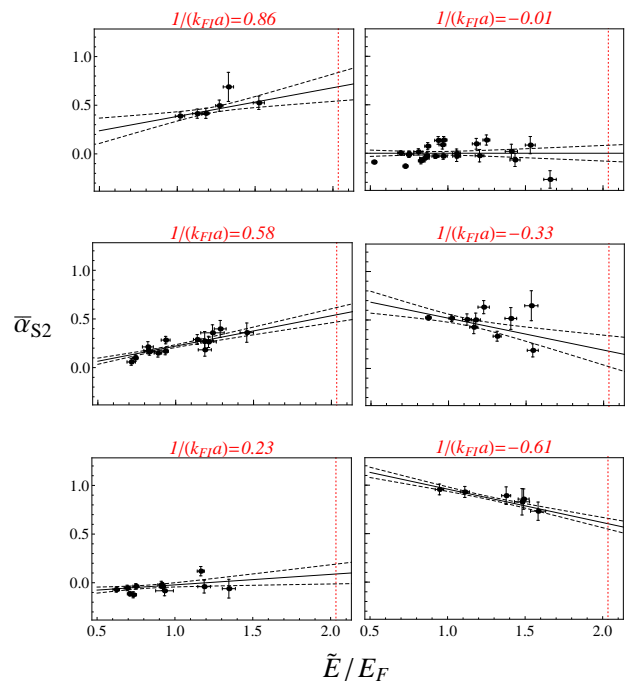


FIG. 4: Scattering length-dependent shear viscosity coefficient $\bar{\alpha}_{S2}$ as a function of energy \tilde{E} and interaction strength $1/(k_{FI}a)$. Black lines denote linear fit to $\alpha_{S2}(\tilde{E})$. Dotted black lines show the range arising from the uncertainty in the straight line fit parameters. Vertical red dotted shows the \tilde{E} where the minimum of $\bar{\alpha}_{S2}$ occurs at $1/(k_{FI}a) = 0$ in Fig. 5.

dependence of $\bar{\alpha}_{S2}$, we determine $\bar{\alpha}_{S2}$ as a function of $1/(k_{FI}a)$ for a given \tilde{E} , as shown in Fig. 5.

For each energy \tilde{E} , the shear viscosity coefficient $\bar{\alpha}_{S2}$ exhibits an approximately parabolic dependence on $1/(k_{FI}a)$, as expected, Fig. 5. Using the linear fits in Fig. 4 to extrapolate to energies above the measured

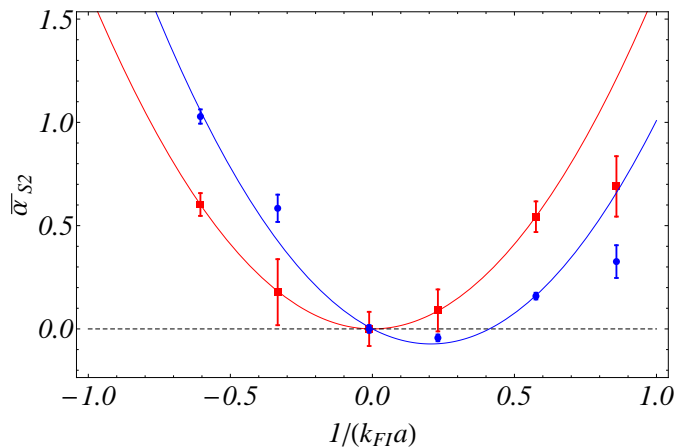


FIG. 5: Shear viscosity coefficient $\bar{\alpha}_{S2}$ versus interaction strength $1/(k_{FI}a)$. Blue circles represent $\bar{\alpha}_{S2}$ obtained from the linear fits in Fig. 4 for an energy $\bar{E}/E_F = 0.8$. The solid blue curve shows a parabolic fit, which has a minimum, slightly negative, value at $1/(k_F a) = 0.21$. Using the linear fits in Fig. 4 to extrapolate to energies above the measured energy range, we obtain the red squares, centered at $1/(k_F a) = 0$ for $\bar{E}/E_F = 2.07$. The red dashed curve shows the corresponding parabolic fit, which is minimized at resonance. Error bars arise from the uncertainty in the linear fit parameters for the data of Fig. 4.

range, we find that a fitted parabola is centered at $1/(k_{FI}a) = 0$ for $\bar{E}/E_F = 2.07$ and has a minimum of zero, as one would expect at high temperatures, where two-body collisions should dominate. Obviously, at still higher energies, the linear fit approximation to the \bar{E} dependence will shift the minimum to the BCS side. However, we expect, but cannot confirm, an asymp-

totic behavior at high energy where the minimum remains at $1/(k_{FI}a) = 0$. In contrast, for lower energy $\bar{E}/E_F = 0.8$, in the range where most of the data is taken, the parabolic fit is centered at $1/(k_{FI}a) = 0.21$ and the minimum $\bar{\alpha}_{S2}$ is slightly negative. We find the same behavior for the energy-averaged $\bar{\alpha}_S$. This suggests that the total shear viscosity coefficient $\bar{\alpha}_S$ has a minimum on the BEC side of resonance in the low energy regime, and that $\bar{\alpha}_{S2}$ contains a term with an odd dependence on $1/(k_{FI}a)$.

Our measurements are consistent with the shear viscosity frequency sum rule [13, 15], which provides a bound on the frequency integrated shear viscosity $\eta(\omega)$. The frequency integral can be written as $p - 3\Delta p$, which is equivalent to $\frac{2}{3}\mathcal{E} - 2\Delta p$. In the high temperature limit, we find $p - 3\Delta p$ contains a term $\propto 1/(k_F a)^2$ and that there are no terms linear in $1/(k_F a)$. In contrast, at low temperature, we find that $\frac{2}{3}\mathcal{E} - 2\Delta p$ contains a term proportional to $-1/(k_F a)$ as well as a quadratic term. Hence, the minimum of the sum rule also is shifted toward the BEC side at low temperature.

This research is supported by the Physics Division of the National Science Foundation (Quantum transport in strongly interacting Fermi gases PHY-1067873), the Division of Materials Science and Engineering, the Office of Basic Energy Sciences, Office of Science, U.S. Department of Energy (Thermodynamics in strongly correlated Fermi gases de-sc0008646), the Physics Divisions of the Army Research Office (Strongly interacting Fermi gases in reduced dimensions W911NF-11-1-0420) and the Air Force Office of Scientific Research (Non-equilibrium Fermi gases FA9550-13-1-0041). The authors are pleased to acknowledge K. Dusling and T. Schäfer, North Carolina State University, for stimulating conversations.

-
- [1] K. M. O'Hara, S. L. Hemmer, M. E. Gehm, S. R. Granade, and J. E. Thomas, *Science* **298**, 2179 (2002).
 - [2] S. Giorgini, L. P. Pitaevskii, and S. Stringari, *Rev. Mod. Phys.* **80**, 1215 (2008).
 - [3] W. Ketterle and M. W. Zwierlein, *Making, probing and understanding ultracold Fermi gases* (IOS Press, Amsterdam, 2008), in *Ultracold Fermi Gases*, Proceedings of the International School of Physics Enrico Fermi, Course CLXIV, Varenna, 20 - 30 June 2006.
 - [4] I. Bloch, J. Dalibard, and W. Zwerger, *Rev. Mod. Phys.* **80**, 885 (2008).
 - [5] A. Adams, L. D. Carr, T. Schäfer, P. Steinberg, and J. E. Thomas, *New J. Phys.* **14**, 115009 (2012).
 - [6] M. Bartenstein, A. Altmeyer, S. Riedl, R. Geursen, S. Jochim, C. Chin, J. H. Denschlag, R. Grimm, A. Simoni, E. Tiesinga, et al., *Phys. Rev. Lett.* **94**, 103201 (2005).
 - [7] L. Luo, B. Clancy, J. Joseph, J. Kinast, and J. E. Thomas, *Phys. Rev. Lett.* **98**, 080402 (2007).
 - [8] L. Luo and J. E. Thomas, *J. Low Temp. Phys.* **154**, 1 (2009).
 - [9] M. Horikoshi, S. Najajima, M. Ueda, and T. Mukaiyama, *Science* **327**, 442 (2010).
 - [10] S. Nascimbène, N. Navon, K. J. Jiang, F. Chevy, and C. Salomon, *Nature* **463**, 1057 (2010).
 - [11] M. Ku, A. T. Sommer, L. W. Cheuk, and M. W. Zwierlein, *Science* (2012).
 - [12] G. M. Bruun and H. Smith, *Phys. Rev. A* **75**, 043612 (2007).
 - [13] E. Taylor and M. Randeria, *Phys. Rev. A* **81**, 053610 (2010).
 - [14] H. Guo, D. Wulin, C.-C. Chien, and K. Levin, *Phys. Rev. Lett.* **107**, 020403 (2011).
 - [15] T. Enss, R. Haussmann, and W. Zwerger, *Annals Phys.* **326**, 770 (2011).
 - [16] P. K. Kovtun, D. T. Son, and A. O. Starinets, *Phys. Rev. Lett.* **94**, 111601 (2005).
 - [17] C. Cao, E. Elliott, J. Joseph, H. Wu, J. Petricka, T. Schäfer, and J. E. Thomas, *Science* **331**, 58 (2011).
 - [18] C. Cao, E. Elliott, H. Wu, and J. E. Thomas, *New J. Phys.* **13**, 075007 (2011).
 - [19] J. E. Thomas, J. Kinast, and A. Turlapov, *Phys. Rev.*

Lett. **95**, 120402 (2005).

- [20] See the supplemental material that is available online.
 [21] E. Elliott, J. A. Joseph, and J. E. Thomas (2013), <http://arxiv:1308.3162v2> [cond-mat.quant-gas].
 [22] T.-L. Ho and E. Mueller, Phys. Rev. Lett. **92**, 160404 (2004).
 [23] D. Guery-Odelin, F. Zambelli, J. Dalibard, and S. Stringari, Phys. Rev. A **60**, 4851 (1999).

Appendix A: Supplemental Material

In this supplemental material, we derive an evolution equation in a scaling approximation for the radii of an expanding cloud as a function of interaction strength near a collisional (Feshbach) resonance. We include viscous forces and heating. We also include the change in the pressure relative to the resonant regime, which breaks conformal symmetry. Finally, we discuss the measurement method.

1. Hydrodynamic Equations

We employ a hydrodynamic description for a single component fluid [17, 18], where the velocity field $\mathbf{v}(\mathbf{r}, t)$ is determined by the scalar pressure and the viscosity pressure tensor,

$$nm(\partial_t + \mathbf{v} \cdot \nabla)v_i = -\partial_i p + \sum_j \partial_j (\eta \sigma_{ij} + \zeta_B \sigma' \delta_{ij}) - n \partial_i U_{total}. \quad (\text{A1})$$

Here p is the scalar pressure and m is the atom mass. U_{total} is the total trapping potential energy arising from the optical trap U_{opt} and the bias magnetic field curvature U_{mag} , as described in the main text. The second term on the right describes the friction forces arising from both shear η and bulk ζ_B viscosities, where $\sigma_{ij} = \partial v_i / \partial x_j + \partial v_j / \partial x_i - 2\delta_{ij} \nabla \cdot \mathbf{v} / 3$ and $\sigma' \equiv \nabla \cdot \mathbf{v}$. Current conservation for the density $n(\mathbf{r}, t)$ requires

$$\frac{\partial n}{\partial t} + \nabla \cdot (n\mathbf{v}) = 0. \quad (\text{A2})$$

Finally, consistent with Eq. A1 and Eq. A2, conservation of total energy is described by

$$\frac{d}{dt} \int d^3\mathbf{r} \left(n \frac{1}{2} m \mathbf{v}^2 + \mathcal{E} + n U_{total} \right) = 0. \quad (\text{A3})$$

The first term in Eq. A3 is the kinetic energy arising from the velocity field and \mathcal{E} is the internal energy density of the gas. As shown below, energy conservation will play an important role in determining a general evolution equation for the cloud radii, both at resonance, where the pressure obeys $p = \frac{2}{3} \mathcal{E}$ and away from resonance, where $\Delta p \equiv p - \frac{2}{3} \mathcal{E} \neq 0$.

For each direction $i = x, y, z$, the mean square size $\langle x_i^2 \rangle \equiv \frac{1}{N} \int d^3\mathbf{r} n(\mathbf{r}, t) x_i^2$ obeys

$$\begin{aligned} \frac{d\langle x_i^2 \rangle}{dt} &= \frac{1}{N} \int d^3\mathbf{r} \frac{\partial n}{\partial t} x_i^2 = \frac{1}{N} \int d^3\mathbf{r} [-\nabla \cdot (n\mathbf{v})] x_i^2 \\ &= \frac{1}{N} \int d^3\mathbf{r} n \mathbf{v} \cdot \nabla x_i^2 = 2\langle x_i v_i \rangle, \end{aligned} \quad (\text{A4})$$

where N is the total number of atoms. We have used integration by parts and $n = 0$ for $x_i \rightarrow \pm\infty$ to obtain the second line. Similarly,

$$\begin{aligned} \frac{d\langle x_i v_i \rangle}{dt} &= \frac{1}{N} \int d^3\mathbf{r} n x_i \frac{\partial v_i}{\partial t} + \frac{1}{N} \int d^3\mathbf{r} \frac{\partial n}{\partial t} x_i v_i \\ &= \frac{1}{N} \int d^3\mathbf{r} n x_i \frac{\partial v_i}{\partial t} + \frac{1}{N} \int d^3\mathbf{r} n \mathbf{v} \cdot \nabla (x_i v_i) \\ &= \langle x_i (\partial_t + \mathbf{v} \cdot \nabla) v_i \rangle + \langle v_i^2 \rangle. \end{aligned} \quad (\text{A5})$$

Combining Eq. A4 and Eq. A5, we obtain,

$$\frac{d^2 \langle x_i^2 \rangle}{dt^2} \frac{1}{2} = \langle x_i (\partial_t + \mathbf{v} \cdot \nabla) v_i \rangle + \langle v_i^2 \rangle. \quad (\text{A6})$$

To proceed, we use Eq. A1, which yields

$$\begin{aligned} \int d^3\mathbf{r} n x_i (\partial_t + \mathbf{v} \cdot \nabla) v_i &= \\ &= \frac{1}{m} \int d^3\mathbf{r} x_i (-\partial_i p - n \partial_i U_{total}) \\ &+ \frac{1}{m} \sum_j \int d^3\mathbf{r} x_i \partial_j (\eta \sigma_{ij} + \zeta_B \sigma' \delta_{ij}) \end{aligned}$$

Integrating by parts on the right hand side, assuming that the surface terms vanish, we obtain

$$\begin{aligned} \langle x_i (\partial_t + \mathbf{v} \cdot \nabla) v_i \rangle &= \frac{1}{Nm} \int d^3\mathbf{r} p - \frac{1}{m} \langle x_i \partial_i U_{total} \rangle \\ &- \frac{1}{Nm} \int d^3\mathbf{r} (\eta \sigma_{ii} + \zeta_B \sigma') \end{aligned} \quad (\text{A7})$$

with $\sigma' \equiv \nabla \cdot \mathbf{v}$. Defining the viscosity coefficients α_S and α_B by $\eta \equiv \alpha_S \hbar n$ and $\zeta_B \equiv \alpha_B \hbar n$, respectively, we can write,

$$\begin{aligned} \langle x_i (\partial_t + \mathbf{v} \cdot \nabla) v_i \rangle &= \frac{1}{Nm} \int d^3\mathbf{r} p - \frac{1}{m} \langle x_i \partial_i U_{total} \rangle \\ &- \frac{\hbar}{m} (\alpha_S \sigma_{ii} + \alpha_B \sigma'), \end{aligned} \quad (\text{A8})$$

where

$$\langle \alpha_S \sigma_{ii} + \alpha_B \sigma' \rangle \equiv \frac{1}{N} \int d^3\mathbf{r} n (\alpha_S \sigma_{ii} + \alpha_B \sigma'). \quad (\text{A9})$$

Using Eq. A8 in Eq. A6, we then obtain for one direction x_i ,

$$\begin{aligned} \frac{d^2 \langle x_i^2 \rangle}{dt^2} \frac{1}{2} &= \frac{1}{Nm} \int d^3\mathbf{r} p + \langle v_i^2 \rangle - \frac{1}{m} \langle x_i \partial_i U_{total} \rangle \\ &- \frac{\hbar}{m} (\alpha_S \sigma_{ii} + \alpha_B \sigma'). \end{aligned} \quad (\text{A10})$$

Eq. A10 determines the evolution of the mean square cloud radii along each axis, $\langle x_i^2 \rangle$, which depends on the conservative forces arising from the scalar pressure and the trap potential, as well as the viscous forces arising from the shear and bulk viscosities.

2. Scaling Solution

We determine the viscosity by measuring the cloud radii and the transverse aspect ratio as a function of time after the cloud is released from the trap. To analyze the aspect ratio data, we employ a scaling solution of Eq. A10, where the density is given by

$$n(\mathbf{r}, t) = \frac{n_0(x/b_x, y/b_y, z/b_z)}{\Gamma}, \quad (\text{A11})$$

where $b_i(t)$, $i = x, y, z$ is a time dependent scale factor, with $b_i(0) = 1$ and $\dot{b}_i(0) = 0$. n_0 is the density profile of the trapped cloud in equilibrium. Here, $\Gamma(t) \equiv b_x b_y b_z$ is the volume scale factor, which is independent of the spatial coordinates in the scaling approximation. With a velocity field that is linear in the spatial coordinates, $v_i = x_i \dot{b}_i / b_i$, Eq. A2 is automatically satisfied.

We note that $\langle x_i^2 \rangle = \langle x_i^2 \rangle_0 b_i^2(t)$, and $\langle v_i^2 \rangle = \langle x_i^2 \rangle_0 \dot{b}_i^2 / b_i^2 = \langle x_i^2 \rangle_0 \dot{b}_i^2(t)$, where $\langle x_i^2 \rangle_0$ is the mean-square cloud radius of the trapped cloud in the i^{th} direction, just before release. Then, with these scaling assumptions, Eq. A10 yields

$$\begin{aligned} \langle x_i^2 \rangle_0 b_i \ddot{b}_i &= \frac{1}{Nm} \int d^3\mathbf{r} p - \frac{1}{m} \langle x_i \partial_i U_{total} \rangle \\ &- \frac{\hbar}{m} \langle \alpha_S \sigma_{ii} + \alpha_B \nabla \cdot \mathbf{v} \rangle. \end{aligned} \quad (\text{A12})$$

We see that Eq. A12 contains the pressure only in a volume integral. To determine the evolution equation for the pressure integral, we write,

$$\frac{1}{N} \int d^3\mathbf{r} p = \frac{2}{3} \frac{1}{N} \int d^3\mathbf{r} \mathcal{E} + \frac{1}{N} \int d^3\mathbf{r} \Delta p, \quad (\text{A13})$$

where we have defined

$$\Delta p \equiv p - \frac{2}{3} \mathcal{E}. \quad (\text{A14})$$

As noted in our previous study of scale invariance [21], Δp is the conformal symmetry breaking pressure change, which vanishes at resonance, where $p = \frac{2}{3} \mathcal{E}$.

Next, we use energy conservation to find the evolution equation for the volume integral of the internal energy density \mathcal{E} from Eq. A3. Analogous to the methods used to derive Eq. A6, we move the time derivatives of the velocity field and density inside the integral in Eq. A3 and use Eq. A1 and Eq. A2 to obtain an evolution equation for the volume integral of the energy density,

$$\frac{d}{dt} \int d^3\mathbf{r} \mathcal{E} + \int d^3\mathbf{r} (\nabla \cdot \mathbf{v}) p + \int d^3\mathbf{r} n \frac{\partial U_{total}}{\partial t} = \dot{Q}, \quad (\text{A15})$$

where $\dot{Q} \equiv \int d^3\mathbf{r} \dot{q}$ is the total heating rate arising from the friction forces and \dot{q} is the heating rate per unit volume,

$$\dot{q} = \frac{1}{2} \eta \sum_{ij} \sigma_{ij}^2 + \zeta_B (\nabla \cdot \mathbf{v})^2, \quad (\text{A16})$$

with the shear viscosity $\eta = \alpha_S \hbar n$ and the bulk viscosity $\zeta_B = \alpha_B \hbar n$, where $\hbar n$ is the natural scale of viscosity.

Just after release of the cloud, the trap potential is constant in time, and the $\partial_i U_{total}$ term in Eq. A15 vanishes. Using Eq. A14, Eq. A15 takes the form

$$\begin{aligned} \frac{d}{dt} \int d^3\mathbf{r} \mathcal{E} + \frac{2}{3} \int d^3\mathbf{r} (\nabla \cdot \mathbf{v}) \mathcal{E} = \\ \dot{Q} - \int d^3\mathbf{r} (\nabla \cdot \mathbf{v}) \Delta p. \end{aligned} \quad (\text{A17})$$

As we intend to explore small deviations from the scale invariant regime, the last term on the right of Eq. A17 can be evaluated using suitable approximations, as discussed below.

With the scaling assumptions, $\nabla \cdot \mathbf{v} = \dot{\Gamma} / \Gamma$, which is independent of the spatial coordinates, and Eq. A17 reduces to

$$\frac{d}{dt} \int d^3\mathbf{r} \mathcal{E} + \frac{2}{3} \frac{\dot{\Gamma}}{\Gamma} \int d^3\mathbf{r} \mathcal{E} = \dot{Q} - \frac{\dot{\Gamma}}{\Gamma} \int d^3\mathbf{r} \Delta p. \quad (\text{A18})$$

Using the integrating factor $\Gamma^{2/3}$, the volume integral of the energy density at time t after release of the cloud is readily obtained in terms of the initial condition $\int d^3\mathbf{r} \mathcal{E}_0$,

$$\begin{aligned} \int d^3\mathbf{r} \mathcal{E} = \\ \frac{\int_0^t dt \Gamma^{2/3} \dot{Q} + \int d^3\mathbf{r} \mathcal{E}_0 - \int_1^{\Gamma(t)} \frac{d\Gamma}{\Gamma^{1/3}} \int d^3\mathbf{r} \Delta p}{\Gamma^{2/3}}, \end{aligned} \quad (\text{A19})$$

where we have used $\Gamma(0) = 1$.

Eq. A19 is a consequence of energy conservation. Although it can be used to determine the evolution of $\int d^3\mathbf{r} p$ in general, it is particularly well-suited to a perturbative treatment of $\Delta p = p - \frac{2}{3} \mathcal{E}$ in the near scale-invariant regime. In that case, we can approximate the time-dependence of the temperature as adiabatic, i.e., $T = T_0 \Gamma^{-2/3}$, where T_0 is the initial temperature of the trapped cloud. Then the volume integral of Δp becomes a known function of time, as discussed below in more detail in § A 2 a.

We eliminate the initial condition $\int d^3\mathbf{r} \mathcal{E}_0$ using $\mathcal{E}_0 = \frac{3}{2} P_0 - \frac{3}{2} \Delta p_0$ and force balance in the trap, which yields

$$\frac{3}{N} \int d^3\mathbf{r} P_0 = \langle \mathbf{r} \cdot \nabla U_{total} \rangle_0. \quad (\text{A20})$$

Here the subscript (0) denotes the initial condition just after release. Then,

$$\frac{1}{N} \int d^3\mathbf{r} \mathcal{E}_0 = \frac{1}{2} \langle \mathbf{r} \cdot \nabla U_{total} \rangle_0 - \frac{3}{2N} \int d^3\mathbf{r} \Delta p_0. \quad (\text{A21})$$

Using Eq. A21 in Eq. A19, the time-dependent volume integral of the pressure, Eq. A13, takes the form,

$$\frac{1}{N} \int d^3 \mathbf{r} p = \frac{\langle \mathbf{r} \cdot \nabla U_{total} \rangle_0}{3 \Gamma^{2/3}} [1 + C_Q(t) + C_{\Delta p}(t)]. \quad (\text{A22})$$

Here, the effect of heating on the pressure integral is given by $C_Q(t)$, which is determined from

$$\dot{C}_Q(t) \equiv \frac{\Gamma^{2/3}(t) \frac{2\dot{Q}}{N}}{\langle \mathbf{r} \cdot \nabla U_{total} \rangle_0}, \quad (\text{A23})$$

with the initial condition $C_Q(0) = 0$. Using Eq. A16 with the velocity field $v_i = x_i \dot{b}_i / b_i$, where $\partial_j v_i = \delta_{ij} \dot{b}_i / b_i$ is spatially constant, it is straightforward to obtain

$$\frac{2\dot{Q}}{N} = \hbar \bar{\alpha}_S \sum_i \sigma_{ii}^2 + 2\hbar \bar{\alpha}_B \frac{\dot{\Gamma}^2}{\Gamma^2}. \quad (\text{A24})$$

The trap averaged-viscosity coefficients, which appear in Eq. A24, are defined by

$$\begin{aligned} \bar{\alpha}_S(a) &\equiv \int d^3 \mathbf{r} \eta / (N \hbar) \\ \bar{\alpha}_B(a) &\equiv \int d^3 \mathbf{r} \zeta_B / (N \hbar). \end{aligned} \quad (\text{A25})$$

In general, the trap-averaged viscosity coefficients are dependent on the scattering length a and are time-dependent, as described in the main text.

In Eq. A24,

$$\frac{\dot{\Gamma}}{\Gamma} = \frac{\dot{b}_x}{b_x} + \frac{\dot{b}_y}{b_y} + \frac{\dot{b}_z}{b_z} \quad (\text{A26})$$

and

$$\sigma_{ii} = 2 \frac{\dot{b}_i}{b_i} - \frac{2}{3} \frac{\dot{\Gamma}}{\Gamma}. \quad (\text{A27})$$

Then,

$$\sum_i \sigma_{ii}^2 = 4 \sum_i \frac{\dot{b}_i^2}{b_i^2} - \frac{4}{3} \frac{\dot{\Gamma}^2}{\Gamma^2}. \quad (\text{A28})$$

The time-dependent Δp term in Eq. A13 and the last two terms in the numerator of Eq. A19 (with Eq. A21) give the net contributions arising from the pressure change,

$$C_{\Delta p}(t) \equiv C_F(t) - C_F(0) - C_p(t), \quad (\text{A29})$$

where

$$C_F(t) \equiv \frac{\Gamma^{2/3}(t) \frac{3}{N} \int d^3 \mathbf{r} \Delta p}{\langle \mathbf{r} \cdot \nabla U_{total} \rangle_0}. \quad (\text{A30})$$

and

$$C_p(t) \equiv \frac{2 \int_1^{\Gamma(t)} \frac{d\Gamma}{\Gamma^{1/3}} \frac{1}{N} \int d^3 \mathbf{r} \Delta p}{\langle \mathbf{r} \cdot \nabla U_{total} \rangle_0}. \quad (\text{A31})$$

With Eq. A22 for the volume integral of the pressure, Eq. A12 yields our central result for the scale factor evolution,

$$\begin{aligned} \ddot{b}_i &= \frac{\bar{\omega}_i^2}{\Gamma^{2/3} b_i} [1 + C_Q(t) + C_{\Delta p}(t)] \\ &\quad - \frac{\hbar \left(\bar{\alpha}_S \sigma_{ii} + \bar{\alpha}_B \frac{\dot{\Gamma}}{\Gamma} \right)}{m \langle x_i^2 \rangle_0 b_i} - \frac{\langle x_i \partial_i U_{mag} \rangle}{m \langle x_i^2 \rangle_0 b_i}. \end{aligned} \quad (\text{A32})$$

In the last term of Eq. A32, note that U_{total} is replaced by the magnetic potential, U_{mag} defined in the main text, as we are interested in expansion of the cloud after the optical part of the potential is extinguished. Further, we have defined the mean ballistic frequency for an arbitrary trapping potential, which need not be harmonic,

$$\bar{\omega}_i^2 \equiv \frac{\langle x_i \partial_i U_{total} \rangle_0}{m \langle x_i^2 \rangle_0} = \frac{\langle \mathbf{r} \cdot \nabla U_{total} \rangle_0}{3m \langle x_i^2 \rangle_0}. \quad (\text{A33})$$

Here, U_{total} is the total trap potential *prior* to release of the cloud. The second form follows from force balance in equilibrium, $\partial_i p + n \partial_i U_{total} = 0$. Multiplying by x_i and integrating by parts requires that $\langle x_i \partial_i U_{total} \rangle_0$ be the same for all directions.

Eq. A32 determines the expansion factors b_i with the initial conditions $b_i(0) = 0$ and $\dot{b}_i(0) = 0$, using the known trap parameters and a suitable approximation for Δp in the off-resonance case. The trap-averaged (generally time-dependent) shear and bulk viscosity coefficients, $\bar{\alpha}_S$ and $\bar{\alpha}_B$ are used as fit parameters, as described in the main text. In the experiments, we determine $\bar{\alpha}_S$ by fitting the predicted aspect ratios to the aspect ratio data, neglecting the much smaller $\bar{\alpha}_B$, as discussed in the main text. The much smaller $\bar{\alpha}_B$ is measured by observing the mean square cloud radius $\langle \mathbf{r}^2 \rangle$, which is a scalar, as a function of time after release, as described in Ref. [21].

a. High Temperature Approximation to Δp

When the bias magnetic field is tuned away from the Feshbach resonance, the pressure deviates from the unitary limit $\frac{2}{3} \mathcal{E}$. In this case, we use for simplicity an estimate of Δp in the high temperature limit [22], where $p - \frac{2}{3} \mathcal{E}$ is given to second order in the fugacity,

$$\Delta p = p - \frac{2}{3} \mathcal{E} = -\frac{\sqrt{2}}{3} n k_B T \left(T \frac{\partial b_2}{\partial T} \right) (n \lambda_T^3), \quad (\text{A34})$$

where $\lambda_T \equiv h / \sqrt{2\pi m k_B T}$ is the thermal wavelength. Here, b_2 is the part of the second virial coefficient that describes the interactions. For the BEC side of resonance, we ignore the change in the molecular population, which is frozen on the short time of the expansion and take

$$b_2(x) = -\frac{sgn[a]}{2} e^{x^2} \text{erfc}(x), \quad (\text{A35})$$

where $\text{erfc}(x) = 1 - \frac{2}{\sqrt{\pi}} \int_0^x dx' e^{-x'^2}$ and $x = \frac{\lambda_T}{|a|\sqrt{2\pi}}$, with a the s-wave scattering length. As Δp causes only a small perturbation to the flow, we make an adiabatic approximation for the temperature, $T = T_0 \Gamma^{-2/3}$, where T_0 is the initial temperature of the trapped cloud. Then, $x = x_0 \Gamma^{1/3}$, where $x_0 = \frac{\lambda_{T_0}}{|a|\sqrt{2\pi}}$. In the high temperature limit, we approximate $E = 3k_B T$ for a harmonically trapped cloud. With $E_F = \frac{\hbar^2 k_{FI}^2}{2m} = (3N)^{1/3} \hbar \bar{\omega}$ the Fermi energy of an ideal gas at the cloud center and k_{FI} the corresponding wavevector, we have

$$\begin{aligned} x &= x_0 \Gamma^{1/3} \\ x_0 &= \frac{\sqrt{6}}{k_{FI}|a|} \left(\frac{E_F}{E} \right)^{1/2}. \end{aligned} \quad (\text{A36})$$

Now, $T \frac{\partial b_2}{\partial T} = -x b_2'/2$, where $b_2'(x) \equiv \text{sgn}[a] f_2'(x)$ with

$$f_2'(x) \equiv \left[\frac{1}{\sqrt{\pi}} - x e^{x^2} \text{erfc}(x) \right]. \quad (\text{A37})$$

Integrating over the trap volume, using the adiabatic approximation for the temperature, and the scaling solution for the density, we obtain

$$\frac{1}{N} \int d^3 \mathbf{r} \Delta p = \frac{\sqrt{2}}{9} \frac{E}{\Gamma^{2/3}} \bar{z} [x b_2'(x)], \quad (\text{A38})$$

where the trap-averaged fugacity for a gaussian density profile is

$$\bar{z} \equiv \frac{1}{N} \int d^3 \mathbf{r} n \left(\frac{n \lambda_{T_0}^3}{2} \right) = \frac{9}{4\sqrt{2}} \left(\frac{E_F}{E} \right)^3. \quad (\text{A39})$$

As the correction terms are small, we can take $E \simeq \tilde{E} \equiv \langle \mathbf{r} \cdot \nabla U_{total} \rangle_0$ in Eq. A38 and Eq. A39.

Then, to evaluate Eq. A29, we use

$$\frac{1}{N} \int d^3 \mathbf{r} \Delta p = \frac{\tilde{E} \sqrt{6}}{4} \left(\frac{E_F}{\tilde{E}} \right)^{7/2} \frac{\Gamma^{-1/3}}{k_{FI} a} f_2'(x). \quad (\text{A40})$$

Here, the time dependence of x is determined by Eq. A36 with $E \rightarrow \tilde{E}$ and $f_2'(x)$ is given by Eq. A37. We have used $\text{sgn}[a]/|a| = 1/a$ to explicitly show that the volume integral of Δp changes sign with the scattering length as the bias magnetic field is tuned across the Feshbach resonance region.

The evolution equation for the scale factors Eq. A32, is then determined by using Eq. A40 in Eq. A30 to obtain

$$C_F(t) = \frac{3\sqrt{6}}{4} \left(\frac{E_F}{\tilde{E}} \right)^{7/2} \frac{1}{k_{FI} a} \Gamma^{1/3} f_2'(x), \quad (\text{A41})$$

where the time dependence of x is determined by Eq. A36. In Eq. A29, we utilize both $C_F(t)$ and $C_F(0)$, where Eq. A41 is evaluated in the limit $t = 0$, where $\Gamma \rightarrow 1$ and $x \rightarrow x_0$.

We evaluate Eq. A31, using $x = \Gamma^{1/3} x_0$ and transform the integral over Γ into an integral over x , yielding the simple form,

$$C_p(t) = \frac{3}{2} \left(\frac{E_F}{\tilde{E}} \right)^3 [b_2(x) - b_2(x_0)]. \quad (\text{A42})$$

We check for consistency between Eq. A32 for the expansion factors in the scaling approximation and the exact evolution equation for the mean square cloud radius $\langle \mathbf{r}^2 \rangle$ given in Ref. [21], which does not assume a scaling solution. By numerically integrating Eq. A32, we find $\langle x_i^2 \rangle = \langle x_i^2 \rangle_0 b_i^2(t)$ for the given Δp , $\bar{\alpha}_S$ and $\bar{\alpha}_B$. We compare the predicted results for $\langle \mathbf{r}^2 \rangle = \sum_i \langle x_i^2 \rangle$ to those obtained by directly integrating the exact evolution equation for $\langle \mathbf{r}^2 \rangle$ [21]. For different shear and bulk viscosities, and for the high temperature approximation Δp , the results precisely coincide. Although neither the heating nor the shear viscosity explicitly appear in the evolution equation for $\langle \mathbf{r}^2 \rangle$, leaving out $C_Q(t)$ in Eq. A32 results in a large discrepancy, as energy conservation is utilized in the derivation of both sets of equations. The good agreement also shows that the Δp corrections to the expansion factors, Eq. A41 and Eq. A42, are consistently evaluated.

3. Measurement of the Shear Viscosity

In the experiments, the shear viscosity at resonance is parameterized by the energy E per atom $E = \langle U \rangle_0 + \frac{1}{2} \langle \mathbf{r} \cdot \nabla U \rangle_0$ [8, 19]. Away from resonance, we employ the scattering length-independent energy scale $\tilde{E} \equiv \langle \mathbf{r} \cdot \nabla U \rangle_0$, as described in the main text. These energies are self-consistently determined from the expanded cloud profile after release from the trap. Using an initial guess for the shear viscosity and energy, Eq. A32 is used to determine the expansion scale factors, which are then used to determine the initial cloud radii in all three directions. Using the measured the trap frequencies, the initial cloud radii in turn yield improved values of $\langle U \rangle_0$ and $\langle \mathbf{r} \cdot \nabla U \rangle_0$, hence E and \tilde{E} . With the improved energy, the process is repeated to refit the shear viscosity coefficient, which then determines improved estimates of the initial cloud radii. This process is repeated until the energies and shear viscosity coefficients converge to the desired precision. Consistency is tested by checking that $\langle x_i \partial_i U \rangle_0$ is the same for all directions $i = x, y, z$, which follows from force balance in the trap for a scalar pressure.

We neglect the bulk viscosity in Eq. A32, which is small compared to the shear viscosity [21]. We also find the the $C_{\Delta p}$ terms has a very small effect on the transverse aspect ratio, as shown in Fig. 6 and Fig. 7, compared to the scattering-length dependent shear viscosity coefficient $\bar{\alpha}_{S2}$. For this reason, we neglect the model-dependent Δp in determining the shear viscosity coefficients and set $C_{\Delta p} = 0$.

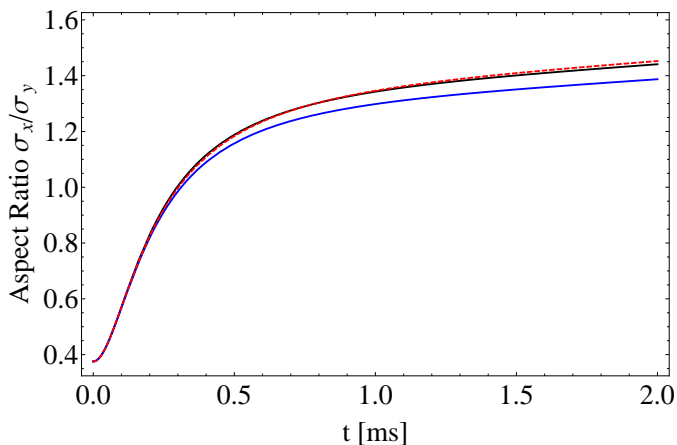


FIG. 6: Transverse aspect ratio σ_x/σ_y for $1/(k_{FI}a) = +0.6$ (above resonance) as a function of time after release, calculated using Eq. A32 with $\tilde{E}/E_F = 1.0$, $\bar{\alpha}_{S0} = 1.2$. Black solid line: $\bar{\alpha}_{S2} = 0$, $C_{\Delta p} = 0$; Red dashed line: $\bar{\alpha}_{S2} = 0$, $C_{\Delta p}$ determined from Eqs. A29, A41, and A42, showing small effect. Blue solid line: $\bar{\alpha}_{S2} = 0.2$, $C_{\Delta p} = 0$.

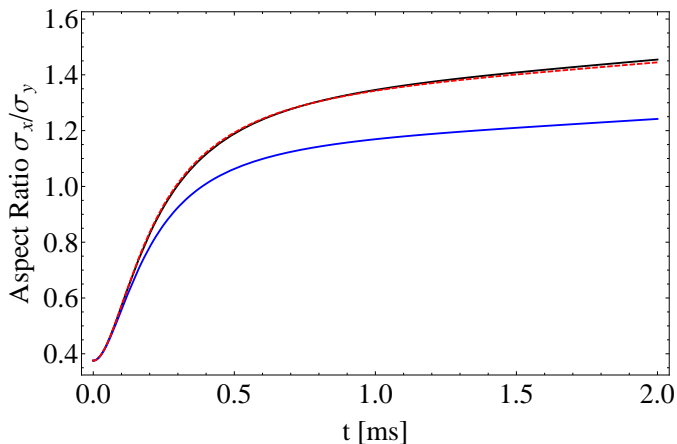


FIG. 7: Transverse aspect ratio σ_x/σ_y for $1/(k_{FI}a) = -0.6$ (below resonance) as a function of time after release, calculated using Eq. A32 with $\tilde{E}/E_F = 1.0$, $\bar{\alpha}_{S0} = 1.2$. Black solid line: $\bar{\alpha}_{S2} = 0$, $C_{\Delta p} = 0$; Red dashed line: $\bar{\alpha}_{S2} = 0$, $C_{\Delta p}$ determined from Eqs. A29, A41, and A42, showing small effect; Blue solid line: $\bar{\alpha}_{S2} = 0.9$, $C_{\Delta p} = 0$.

As described in the main text, we measure the scattering-length-dependent shear viscosity coefficient, $\bar{\alpha}_{S2}$, for six different values of $1/(k_{FI}a) = -0.61, -0.33, -0.01, 0.23, 0, 0.58, 0.86$ and a range of energies \tilde{E} . For each $1/(k_{FI}a)$, we perform a linear fit to the measured energy dependence of $\bar{\alpha}_{S2}(\tilde{E})$. Using these linear fits, we are able to extrapolate the value $\bar{\alpha}_{S2}$ for each $1/(k_{FI}a)$ at a fixed \tilde{E} . The resulting data for

$\bar{\alpha}_{S2}(1/(k_{FI}a))$ for each \tilde{E} is then fit with

$$\bar{\alpha}_{S2}(\tilde{E}) = d_1 \frac{1}{k_{FI}a} + d_2 \frac{1}{(k_{FI}a)^2}, \quad (\text{A43})$$

excluding the $1/(k_{FI}a) = 0.86$ data, for which the expansion is not likely to be valid. The fit coefficients, $d_1(\tilde{E})$ and $d_2(\tilde{E})$, are shown in Fig. 8. We note that the coefficient d_2 is nearly independent of energy, while the coefficient d_1 decreases in magnitude with increasing energy, over the energy range $0.5 < \tilde{E}/E_F < 2$ for which the viscosity was measured.

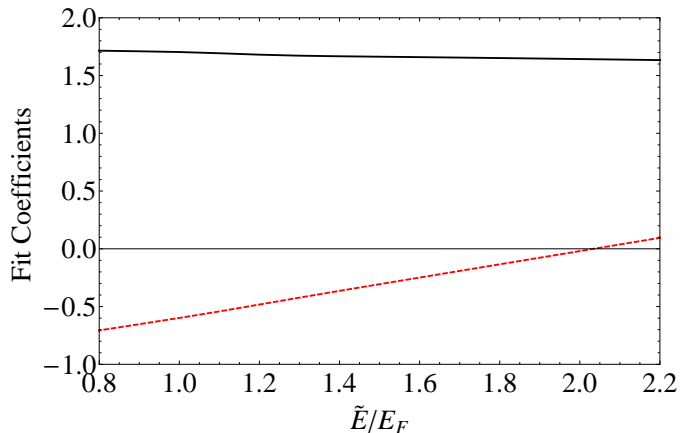


FIG. 8: Coefficients d_1 of $1/(k_{FI}a)$ (bottom dashed line) and d_2 of $1/(k_{FI}a)^2$ (top solid line) versus energy \tilde{E} .

We can compare the shear viscosity coefficients presented in this paper for the energy range $0.5 < E/E_F < 2$, which are measured from the expansion of the transverse aspect ratio, to those obtained in our previous experiments, which were based on collective mode damping [17, 18] and measured for a comparable energy range, Fig. 9. We find that the collective mode damping measurements are systematically larger, except at the lowest energies. In the collective mode damping measurements, we believe that as the cloud energy is increased, the local thermalization rate eventually becomes smaller than the collective mode frequency and the system tends to become ballistic, increasing the damping rate [23].

a. Shear Viscosity at Resonance versus Reduced Temperature

In the main text, the trap-averaged shear viscosity coefficient at resonance is given as a function of the energy per particle E/E_F . This data also can be displayed as a function of the reduced temperature at the trap center $\theta_0 \equiv T_0/T_F(n_0)$, where n_0 is the density at the trap center and T_0 is the temperature of the cloud, prior to release from the trap. We obtain T_0/T_{FI} from

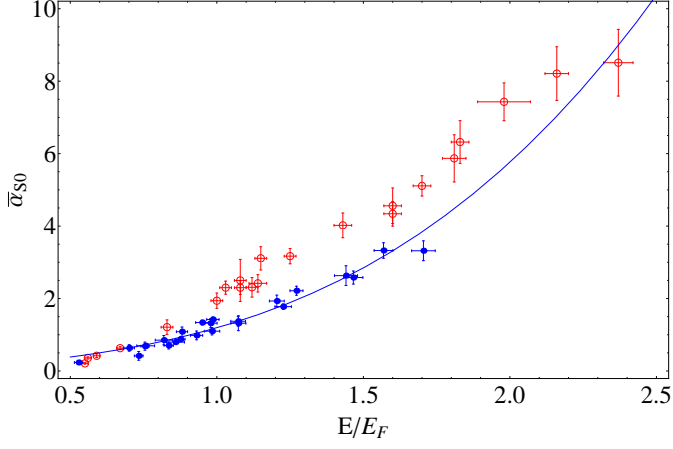


FIG. 9: Shear viscosity coefficient $\bar{\alpha}_{S0}$ for a resonantly interacting Fermi gas versus energy. Blue solid circles from measurement of the transverse aspect ratio versus time after release (this paper). Pink open circles from collective mode damping, Ref. [17, 18]. The solid curve shows the fit $0.63 E/E_F + 0.56 (E/E_F)^3$, as discussed in the main text.

the energy data by using the temperature calibration of Ref. [18], where T_{FI} is the Fermi temperature of an ideal

gas with density n_I at the trap center. Using the ratio $T_F(n_I)/T_F(n_0) = (n_I/n_0)^{2/3}$, we obtain the data shown in Fig. 10.

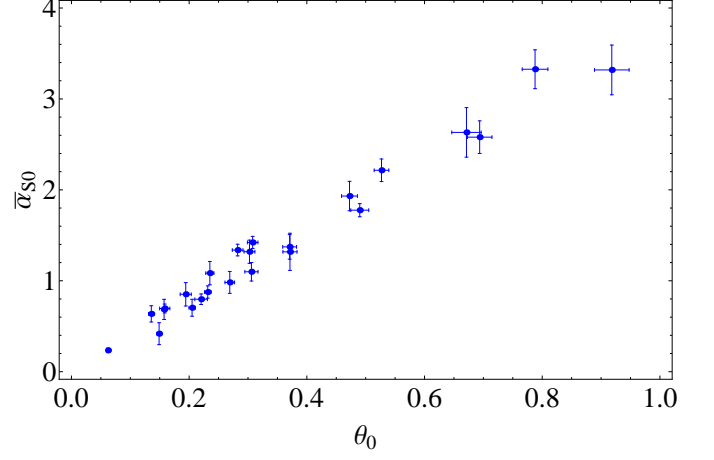


FIG. 10: Shear viscosity coefficient $\bar{\alpha}_{S0}$ for a resonantly interacting Fermi gas versus reduced temperature θ_0 at the trap center.